molecules

MDPI

Article

Adenosine Receptor Ligands: Coumarin–Chalcone Hybrids as Modulating Agents on the Activity of *h*ARs

Saleta Vazquez-Rodriguez [1,*,†], Santiago Vilar [1], Sonja Kachler [2], Karl-Norbert Klotz [2], Eugenio Uriarte [1,3], Fernanda Borges [4] and Maria João Matos [1,4,*]

1 Departamento de Química Orgánica, Facultad de Farmacia, Universidad de Santiago de Compostela, 15782 Santiago de Compostela, Spain; qosanti@yahoo.es (S.V.); eugenio.uriarte@usc.es (E.U.)
2 Institut für Pharmakologie und Toxikologie, Universität Würzburg, 97078 Würzburg, Germany; sonja.kachler@toxi.uni-wuerzburg.de (S.K.); klotz@toxi.uni-wuerzburg.de (K.-N.K.)
3 Instituto de Ciencias Químicas Aplicadas, Universidad Autónoma de Chile, 7500912 Santiago, Chile
4 CIQUP/Department of Chemistry and Biochemistry, Faculty of Sciences, University of Porto, Rua Campo Alegre 687, 4169-007 Porto, Portugal; mfernandamborges@gmail.com
* Correspondence: saleta.vazquezrodriguez@cmd.ox.ac.uk (S.V.-R.); mariajoao.correiapinto@usc.es or maria.matos@fc.up.pt (M.J.M.)
† Current address SVR: Target Discovery Institute, University of Oxford, NDM Research building, Old Road Campus, Oxford OX3 7FX, UK.

Academic Editor: Pascal Richomme
Received: 27 August 2020; Accepted: 18 September 2020; Published: 19 September 2020

Abstract: Adenosine receptors (ARs) play an important role in neurological and psychiatric disorders such as Alzheimer's disease, Parkinson's disease, epilepsy and schizophrenia. The different subtypes of ARs and the knowledge on their densities and status are important for understanding the mechanisms underlying the pathogenesis of diseases and for developing new therapeutics. Looking for new scaffolds for selective AR ligands, coumarin–chalcone hybrids were synthesized (compounds **1**–**8**) and screened in radioligand binding (hA$_1$, hA$_{2A}$ and hA$_3$) and adenylyl cyclase (hA$_{2B}$) assays in order to evaluate their affinity for the four human AR subtypes (hARs). Coumarin–chalcone hybrid has been established as a new scaffold suitable for the development of potent and selective ligands for hA$_1$ or hA$_3$ subtypes. In general, hydroxy-substituted hybrids showed some affinity for the hA$_1$, while the methoxy counterparts were selective for the hA$_3$. The most potent hA$_1$ ligand was compound **7** (K_i = 17.7 μM), whereas compound **4** was the most potent ligand for hA$_3$ (K_i = 2.49 μM). In addition, docking studies with hA$_1$ and hA$_3$ homology models were established to analyze the structure–function relationships. Results showed that the different residues located on the protein binding pocket could play an important role in ligand selectivity.

Keywords: coumarin; chalcone; neurodegenerative diseases; adenosine receptors; binding affinity; docking

1. Introduction

Adenosine receptors (ARs) are cell membrane receptors, belonging to the G protein-coupled receptor (GPCRs) superfamily. ARs comprised of four different subtypes: A$_1$, A$_{2A}$, A$_{2B}$ and A$_3$ [1]. Adenosine is a purine nucleoside and an endogenous modulator of several physiological processes [1–4]. Extracellular adenosine activates the G$_i$-coupled receptors of the A$_1$ and A$_3$ subtypes, depressing the action of the brain, heart, kidneys, and the immune system, amongst other systems, as a consequence of the inhibition of adenylyl cyclase [5]. The A$_3$ subtype of AR has been cloned [6,7], making it possible to establish its pharmacological [8–11] and regulatory features [12].

Due to their widespread presence in cells, ARs proved to be promising targets in drug discovery. During the last decade, the search for selective ligands has been raised [13–15]. Several AR antagonists appeared as promising drug candidates for different pathological processes such as inflammation (A_3) [14], heart and renal failure (A_1) [16], or neurological disorders including Parkinson [17,18] and Alzheimer's diseases (A_{2A} and/or A_1) [19]. ARs can work as targets for various diseases and can open a new window for new therapeutic approaches.

In particular, A_1 antagonists are effective as diuretic agents [20,21] and also show neuroprotective activity in animal models of in vivo ischemia [22]. On the other hand, A_3 antagonists are being investigated as potential agents against renal injury [23] and also as neuroprotective agents [24,25], while A_3 agonists are also under consideration for treating conditions of the central nervous system (CNS) and peripheral nervous system [26,27].

From the arsenal of molecules presenting high potency and selectivity on ARs, the xanthine scaffold was the first to be used to develop the so-called classical AR antagonists [28,29]. In the search for non-xanthine AR ligands, numerous structures were discovered over the years. Flavones and isoflavones have played a remarkable role. As an example, genistein, was described as a competitive antagonist at A_1 in FRTL (thyroid) cells [30], and galangin was found to bind to the three subtypes of ARs displaying micromolar affinity for the A_3 [31]. The affinity of flavonoids and other phytochemicals to ARs brings about the hypothesis that probably other types of natural substances, namely those present in the diet, can interact with this type of receptor.

Coumarins (chromone isosteres) and chalcones (a flavonoid precursor) are naturally occurring benzopyran-related molecules presenting a variety of pharmacological activities [32–34]. Having in mind that both the coumarin and chalcone nuclei are structurally close to flavonoids, the design of novel AR ligands based on their scaffolds emerged as an interesting idea. Our study was also motivated by the structural similarity between the coumarin and the chromone scaffolds, which were previously described as AR ligands [35,36], and by the similarities with some coumarin derivatives previously described in our group [37–42]. In this context, we focused our attention on the 3-benzoylcoumarin core, considered as a hybrid scaffold in which the chalcone is fixed in a *trans* conformation through the double bond of the pyrone ring of the coumarin skeleton (Figure 1), presenting a more restricted conformation compared to the previously described coumarin–chalcone hybrids [36].

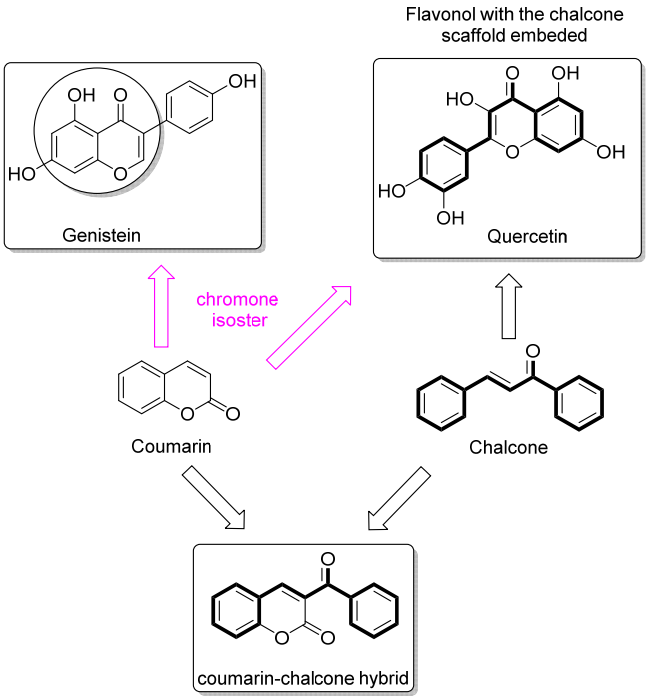

Figure 1. Rational design of coumarin–chalcone hybrids.

Therefore, based on the structural similarities between flavones, chalcones and coumarins, we decided to design and synthesize a novel family of coumarin–chalcone hybrid derivatives and study their activity on the different subtypes of human AR.

2. Results and Discussion

2.1. Chemistry

Two sets of coumarin–chalcone hybrids have been synthesized: one decorated with methoxy substituents (**1**–**4**) and another with hydroxy substituents (**5**–**8**). An efficient and versatile Knoevenagel reaction, treating a commercially available salicylaldehyde and the corresponding methoxylated ethyl benzoylacetate with piperidine in ethanol (EtOH) at reflux for 2–6 h, allowed the desired methoxy-3-benzoylcoumarins **1**–**4** with 85–97% yield. The hydroxy-3-benzoylcoumarins **5**–**8** were obtained by hydrolysis of the corresponding methoxy derivatives, with 75–94% yield, by employing boron tribromide (BBr_3) as deprotecting reagent in dichloromethane (DCM) at 80 °C in a Schlenk tube for 48 h [43]. The synthetic approach is illustrated in Scheme 1 and described in the methods and materials section.

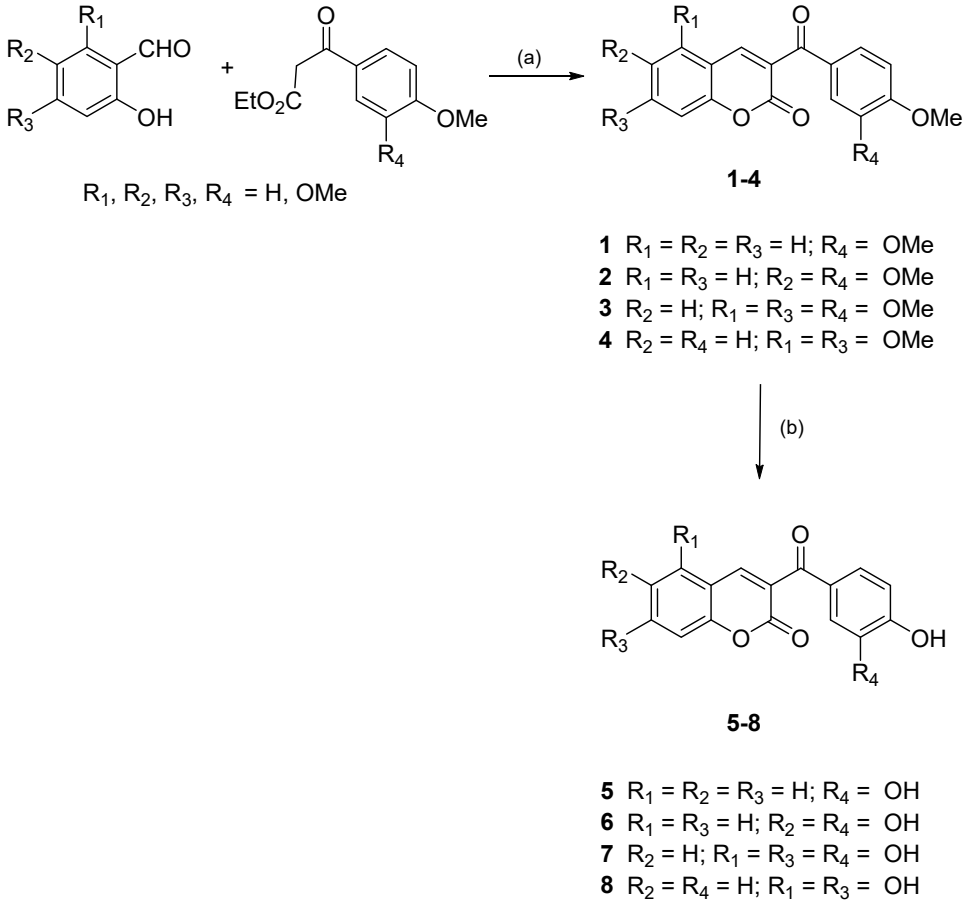

Scheme 1. Synthetic route to obtain the coumarin-chalcone hybrids. *Reagents and conditions:* (**a**) piperidine, EtOH, reflux, 2–6 h; (**b**) BBr_3, DCM, 80 °C, 48 h.

2.2. Pharmacology

Adenosine Receptor Binding Affinity Assays

The adenosine binding affinity of derivatives **1**–**8** for the human AR subtypes hA_1, hA_{2A} and hA_3, expressed in Chinese Hamster Ovary (CHO) cells, was determined in radioligand

competition experiments [43,44]. In the binding affinity assay, it is measured the competition of ligands for specific binding of [^{3}H]CCPA (2-chloro-N^6-cyclopentyladenosine) to hA$_1$; specific binding of [^{3}H]NECA (5′-*N*-ethylcarboxamidoadenosine) to hA$_{2A}$; and specific binding of [^{3}H]HEMADO (2-(1-hexynyl)-N^6-methyladenosine) to hA$_3$. The results are expressed as K_i (dissociation constants), which were calculated with the program SCTFIT, and given as geometric means of at least three experiments, including 95% confidence intervals. Due to the lack of a suitable radioligand for the hA$_{2B}$ receptor, the potency of antagonists at the hA$_{2B}$ receptor was determined by inhibition of NECA-stimulated adenylyl cyclase activity with increasing concentrations of antagonist [43,44]. As a result, cAMP (cyclic adenosine monophosphate) production was inhibited in a concentration-dependent fashion, and K_i values were calculated from the measured IC_{50} values [45].

Derivatives **1**–**8** were efficiently synthesized and their in vitro binding affinity for human AR subtypes hA$_1$, hA$_{2A}$, hA$_{2B}$ and hA$_3$, expressed in CHO cells, was evaluated. In the present communication, the studies were focused on the inspection of the effect on the binding affinity of different number and position of methoxy or hydroxy substituents on the 3-benzoylcoumarin scaffold. Data obtained for the binding affinity for hA$_1$ and hA$_3$ is summarized in Table 1. For all the tested compounds, no significant affinity was detected for the hA$_{2A}$ (Ki > 100 μM) or hA$_{2B}$ (K_i > 10 μM).

Table 1. Binding affinity (K_i) of compounds **1**–**8** on hA$_1$ and hA$_3$ AR.

Compound	hA$_1$ (K_i μM) [a]	hA$_3$ (K_i μM) [a]
1	>100	>100
2	>100	>100
3	>30 [b]	9.03 (6.28–13.0)
4	>100	2.49 (2.33–2.66)
5	39.5 (25.3–61.5)	34.5 (29.7–40.1)
6	54.0 (49.8–58.5)	>60 [b]
7	17.7 (16.0–19.5)	>30 [b]
8	29.1 (20.4–41.5)	>60 [b]
Theophylline	6.77 (4.07–11.3)	86.4 (73.6–101)

[a] Results are geometric means of 3 experiments and given with 95% confidence intervals (in parentheses). [b] At higher concentrations, the compounds precipitate.

The binding affinity results show that derivatives **1** and **2**, without substitutions on the coumarin scaffold or with a single methoxy group at the position 6 of the coumarin core, respectively, display no detectable binding affinity for the evaluated receptors (K_i > 100 μM). However, the presence of two methoxy groups at positions 5 and 7 (compounds **3** and **4**, respectively) lead to an increment on both the potency and selectivity for the hA$_3$. Compound **3**, presenting three methoxy groups at positions 5, 7 and 4′ proved to be hA$_3$ selective, displaying a K_i = 9.03 μM, whereas compound **4**, presenting an extra methoxy groups at position 3′ is not only selective for hA$_3$, but also displays a increase in potency (K_i = 2.49 μM). Compared to theophylline, classically used as a reference compound, we would like to highlight that both compounds **3** and **4** are more potent and hA$_3$ selective molecules.

Based on this data, it can be concluded that both nature and position of the substitution patterns on the coumarin–chalcone scaffold play a key role in the interaction with the hA$_3$. It can be highlighted that positions 5 and 7 of the studied scaffold seem to be relevant for the observed selectivity and potency. Analyzing the methoxylated derivatives **1**–**4**, only the molecules presenting substituents at these two positions (compounds **3** and **4**) are hA$_3$ active and selective ligands.

Interestingly, a similar tendency was observed for hA$_1$ binding of the hydroxylated derivatives (**5**–**8**), which bear hydroxy groups instead of methoxy groups at positions 5 and 7 (compounds **7** and **8**). Derivatives **7** and **8** display the highest potency and selectivity of the studied series towards hA$_1$, but their activity towards this receptor is still low with K_i = 17.7 μM and K_i = 29.1 μM, respectively.

2.3. Theoretical Evaluation of ADME Properties

In order to explore the drug-like properties of compounds **1**–**8**, the lipophilicity, expressed as the octanol/water partition coefficient and herein named clogP, as well as other theoretical calculations such as number of hydrogen acceptors and number of hydrogen bond donors, and topological polar surface area (TPSA), were calculated using the Molinspiration software [46]. Theoretical prediction of absorption, distribution, metabolism and excretion (ADME) properties of all derivatives is summarized in Table 2.

Table 2. Theoretical evaluation of the ADME properties of coumarin–chalcone hybrids.[a]

Compound	clogP	TPSA (Å^2)	*n*-OH Acceptors	*n*-OHNH Donors	Volume (Å^3)
1	3.04	65.75	5	0	270.07
2	3.08	74.98	6	0	295.62
3	3.06	84.22	7	0	321.16
4	3.47	74.98	6	0	295.16
5	2.43	87.74	5	2	235.01
6	1.93	107.97	6	3	243.03
7	1.63	128.20	7	4	251.05
8	2.12	107.97	6	3	243.03

[a] TPSA, topological polar surface area; n-OH, number of hydrogen acceptors; n-OHNH, number of hydrogen bond donors.

Based on this theoretical data, it can be concluded that the study molecules **1**–**8** do not violate any of Lipinski's rules (namely molecular weight, clogP, number of hydrogen donors and acceptors). In addition, TPSA, described as an indicator of membrane permeability, was favorable for the studied compounds.

2.4. Molecular Modeling

hA$_1$ and hA$_3$ homology models were successfully constructed (Materials and methods section). A selection of models obtained from Induce Fit calculations were tested based on their ability to discriminate between known ligands, decoys and between subtype-selective compounds. The models selected for the docking calculations showed excellent results in both tests. A dataset of 200 randomly selected decoys from the ZINC database [47] were mixed up with 22 known ligands of each adenosine receptor subtype [48] Glide SP precision was used to dock the database to the hA$_1$ and hA$_3$ models [49]. Table 3 presents the area under the receiver operating characteristic (ROC) curve (AUROC) for both systems. To differentiate between subtype-selective ligands, a second and more challenging test was performed. As in a previous study [48], 66 subtype-selective molecules (22 hA$_1$, 22 hA$_{2A}$ and 22 hA$_3$ compounds) were docked to the hA$_1$ model (22 true positives vs. 44 false positives) and to the hA$_3$ (22 true positives vs. 44 false positives). Results corroborate those previously published by Katritch et al. [50] and proved that the developed homology models are able to discriminate between subtype-selective compounds (Table 3).

Table 3. Area under the ROC curve (AUROC) for the two homology models.

AUROC	hA$_1$	hA$_3$
test 1 [a]	0.91	0.95
test 2 [b]	0.86	0.82

[a] 22 hA$_1$ or 22 hA$_3$ ligands as true positives (TP) and 200 random decoys as false positives (FP) were considered. [b] For hA$_1$, 22 hA$_1$ selective compounds as TP and 22 hA$_{2A}$ + 22 hA$_3$ compounds as FP were considered. For hA$_3$, 22 hA$_3$ compounds as TP and 22 hA$_{2A}$ + 22 hA$_1$ compounds as FP were considered.

Glide SP molecular docking simulations were run with our data using the hA$_1$ and hA$_3$ selected homology models as protein structures to detect the hypothetical binding mode of the new synthesized compounds [51]. The Prime module was used to optimize the protein structure for each binding mode [52]. Molecular docking simulations are represented in Figure 2.

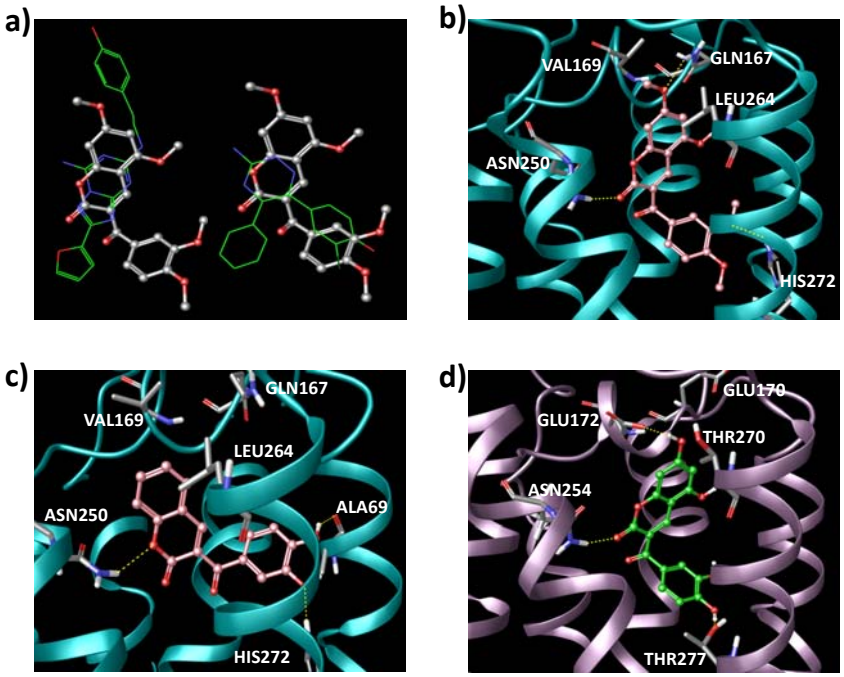

Figure 2. (**a**) Comparative study of the co-crystallized ligands (green carbons) in the hA$_{2A}$ [3EML (left) and 3UZC (right)] with the pose of compound **3** extracted from the hA$_3$ docking calculations (grey carbons). Binding pockets in hA$_{2A}$ and hA$_3$ were superposed. (**b**) Pose extracted for compound **3** inside the hA$_3$ after docking. Hydrogen bonds are represented in yellow color. (**c**) Hypothetical binding mode for compound **5** (pink carbons) in the hA$_3$. (**d**) Pose obtained through docking simulations for compound **7** (green carbons) in the hA$_1$ protein pocket.

Docking calculations and the established homology models for the hA$_1$ and hA$_3$ identified the hypothetical binding mode and rationalized the interaction of these derivatives with their respective ARs binding sites.

The calculations showed a high level of variability since all the synthetized derivatives yielded different possible binding modes inside the pockets. Selection of the hypothetical binding pose was accomplished considering the number of similar poses extracted from the simulations and geometrical correspondence to crystallized ligands in the hA$_{2A}$ (Figure 2a).

Docking results disclosed important data about the binding mode: the oxygens presented in the benzopyrone system are oriented towards the Asn250 residue and the benzoyl moiety was buried in the hA$_3$ pocket. This hypothetical binding mode corroborates the conformations shown by the co-crystallized ligands in the hA$_{2A}$ (PDB: 3EML and 3UZC) [48,53] (Figure 2a,b). The pose of compound **3** produced effective hydrogen bonds with Gln167, Asn250 and His272 residues.

Interestingly, when methoxy substituents were demethylated and changed into hydroxy equivalents (compounds **5**–**8**) a modification in the profile of the studied derivatives was noticed: a loss of affinity for hA$_3$ and a tendency for interaction with hA$_1$. The only compound that discloses some affinity for both receptors was compound **5** (hA$_1$ K_i = 39.5 and hA$_3$ K_i = 34.5 μM), which presents a catechol at positions 3′ and 4′ and no substitutions in the coumarin fragment. The hypothetical binding mode for compound **5** in the hA$_3$ pocket is represented in Figure 2c. The compound can establish hydrogen bonds with Ala69, Asn250 and His272 residues. As observed in the hA$_{2A}$ crystallized

structure and previously published studies [54,55], the corresponding Asn250 residue seems to play an important role in ligand recognition. The compound **5** pose inside the hA_1 pocket is likewise the described pose in the hA_3 one. However, the position was slightly shifted, and calculations were not able to retrieve a hydrogen bond with the Asn250 residue. The introduction of an additional hydroxy group at position 6 of the coumarin scaffold (compound **6**), resulted in a loss of measurable hA_3 binding affinity. The most noticeable binding affinities were found for derivatives with hydroxy substitutions at positions 5 and 7 of the coumarin core, as stated for methoxy equivalents. Thereby, compound **7**, with the same substitution pattern as quercetin (Figure 1), that is, hydroxy groups at positions 5, 7, 3′ and 4′, displays hA_1 selectivity, and the best binding affinity (K_i = 17.7 μM). Compound **8**, with the same substitution pattern as genistein (Figure 1, hydroxy substituents at positions 5, 7 and 4′) shows a similar hA_1 selectivity (K_i = 29.1 μM). The pose obtained through docking calculations for compound **7** in the hA_1 protein pocket showed the possibility of establishment of hydrogen bonds with Glu172, Asn254 and Thr277 residues (Figure 2d).

Moreover, we calculated the interaction energy contributions of the residues in hA_3 and hA_1 pockets with compounds **3** and **7**, respectively (Figure 3). The sum of different individual contributions, such as Coulomb, *van der Waals* and hydrogen bond energies, was taken into account in the calculation of the interaction energies for each residue.

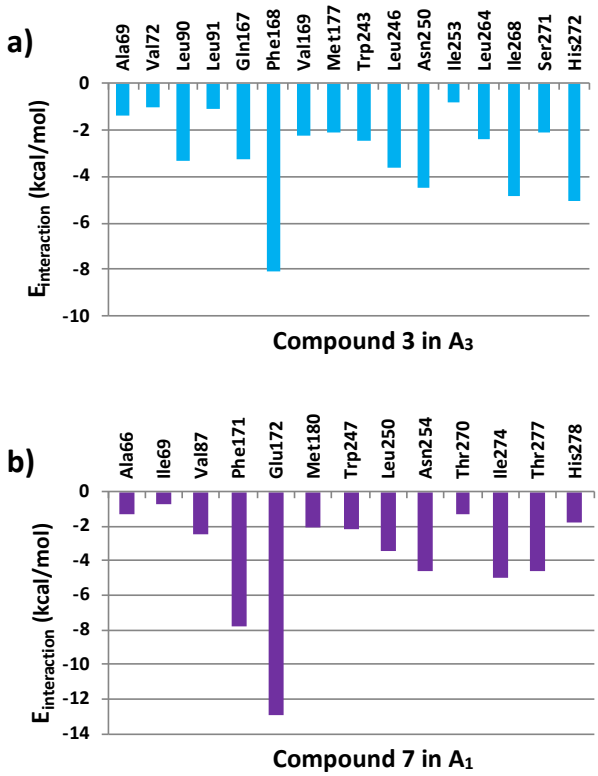

Figure 3. Interaction energy contribution (sum of Coulomb, *van der Waals* and hydrogen bond energies) between the residues in the (**a**) hA_3 and (**b**) hA_1 and the respective derivatives **3** and **7** (residues in a distance of 3 Å from the ligand).

In addition, Figure 4 shows the molecular surface around the two residues in the hA_1 and hA_3 that could be responsible for the observed selectivity.

Regarding the interaction energy contributions (Figure 4), calculations showed that the molecular surface around the two residues in the hA_1 and hA_3 could be responsible for the observed selectivity. Phe168, Asn250, Ile268 and His272 are important residues in the interaction between compound **3** and the hA_3. Residues with important contributions in the stabilization of compound **7** inside the hA_1 are Phe171, Gln172, Asn254, Ile274 and Thr277.

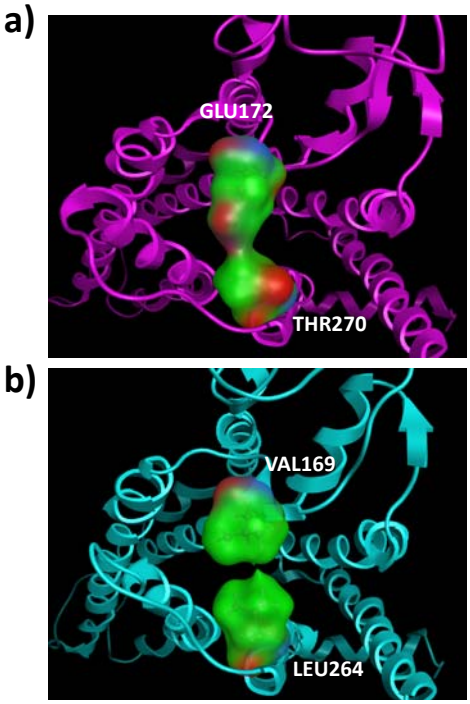

Figure 4. Molecular surface showing favored interaction areas generated in the (**a**) hA$_1$ and (**b**) hA$_3$. Red color represents hydrogen-bond areas, green color shows hydrophobic areas, and blue represents mildly polar interfaces. Protein structures are viewed from the extracellular side.

There are different residues in both hA$_1$ and hA$_3$ with different hydrophobic/hydrophilic characteristics, which may be important to understand the observed selectivity. Hydrophobic residues in the hA$_3$, such as Val169 and Leu264, could establish hydrophobic interactions and contribute towards stabilizing the ligand when the derivatives present hydrophobic substituents, like methoxy groups (i.e., **3** and **4**) (Figure 4). However, in the case of hA$_1$, the corresponding residues are Glu172 and Thr270. They have hydrophilic characteristics and so can stabilize the binding of derivatives with polar substituents, such as the hybrids with hydroxy groups (compounds **6**–**8**). Yet, compound **5,** with no substituents in the coumarin ring, can be stabilized in the pocket of both proteins.

3. Materials and Methods

3.1. Chemistry

3.1.1. General Methods

Starting materials and reagents were obtained from commercial suppliers and were used without purification. Melting points (mp) were determined using a Reichert Kofler thermopan or in capillary tubes on a Büchi 510 (Flawil, Switzerland) apparatus and were uncorrected. ^{1}H-NMR (300 MHz) and ^{13}C-NMR (75.4 MHz) spectra were recorded with a Bruker AMX spectrometer (Bruker Daltonics Inc., Fremont, CA, USA) using DMSO-d_6 or $CDCl_3$ as solvent. Chemical shifts (δ) are expressed in parts per million (ppm) using TMS as an internal standard. Coupling constants J are expressed in hertz (Hz). Spin multiplicities are given as s (singlet), bs (broad singlet), d (doublet), dd (doublet of doublets) and m (multiplet). Mass spectrometry was carried out with a Kratos MS-50 or a Varian MAT-711 spectrometer (Thermo Fisher Scientific, Waltham, MA, USA). Elemental analyses were performed by a Perkin–Elmer 240B microanalyzer (Thermo Fisher Scientific, Waltham, MA, USA) and were within ±0.4% of the calculated values in all cases. The analytical results were ≥95% purity for all compounds. Flash Chromatography (FC) was performed on silica gel (Merck 60, 230–400 mesh,

Kenilworth, NJ, USA) and analytical TLC on precoated silica gel plates (Merck 60 F254, Kenilworth, NJ, USA). Organic solutions were dried over anhydrous sodium sulfate. Concentration and evaporation of the solvent after reaction or extraction was carried out on a Büchi rotavapor (BÜCHI Labortechnik AG, Switzerland) operating at reduced pressure. The purity of compounds was assessed by high performance liquid chromatography (HPLC) coupled at diode array detector (DAD) on a Thermo Quest Spectrasystem (Thermo Fisher Scientific, Waltham, MA, USA) equipped with a P4000 pump, an UV6000 UV-Vis diode array detector, and a SN4000 interface to be operated via a personal computer. The instrument software ChromQuest 5.0 (Thermo Fisher Scientific, Waltham, MA, USA) was used for data acquisition. Different analytical columns and mobile phases (all solvents were HPLC grade) were tested. The mobile phase was H_2O:CH_3CN = 70:30 and an Eclipse xdb C18 column (5 μm particle size, 0.46 mm i.d., 25 cm length; Agilent Technologies, CA, USA) was used. The purity of the compounds was found to be higher than 95%.

3.1.2. Synthetic Protocol to Obtain the Methoxy-3-benzoylcoumarins **1**–**4**

To a solution of the appropriate *β*-ketoester (1 mmol) and the corresponding salicylaldehyde (1 mmol) in ethanol (5 mL) piperidine in catalytic amount (0.10 mL) was added. The reaction mixture was refluxed for 2–6 h and, after completion (followed by TLC), the reaction was cooled, and the precipitate was filtered and washed with cold ethanol and ether. The obtained solid was recrystallized in DCM to afford the corresponding methoxy-3-benzoylcoumarin compounds.

3.1.3. Synthetic Protocol to Obtain the Hydroxy-3-benzoylcoumarins **5**–**8**

In a Schlenk tube, the appropriate methoxy derivative compound **1**–**4** (1 mmol) was dissolved in DCM (1 mL), and BBr_3 (20 mmol, 1M) was added dropwise. The tube was sealed, and the reaction mixture was heated at 80 °C for 48 h. The resulting crude product was treated with MeOH and rotated to dryness. The obtained crude solid was recrystallized in MeOH or purified by flash chromatography using hexane/ethyl acetate mixtures as eluent, to afford the desired hydroxy derivatives.

3-(3′,4′-Dimethoxybenzoyl)coumarin (**1**): 85% yield; white solid; mp 190–191 °C; ^{1}H-NMR (300 MHz, $CDCl_3$) δ ppm 8.01 (s, 1H, H-4), 7.71–7.52 (m, 3H, 3x Ar-H), 7.50–7.29 (m, 3H, 3x Ar-H), 6.87 (d, *J* = 8.4 Hz, 1H, H-5′), 3.95 (s, 6H, 2x OCH_3); ^{13}C-NMR (75 MHz, $CDCl_3$) δ ppm 190.3, 154.8, 154.4, 149.5, 144.6, 133.6, 129.3, 129.2, 127.8, 125.7, 125.2, 118.5, 117.2, 111.2, 110.2, 56.4, 56.3; EI-MS *m*/*z* (%): 311 ([M + 1]$^+$, 59), 310 (M$^+$, 100), 173 (41), 166 (25), 165 (99), 79 (22), 77 (22); Anal. Calcd. For $C_{18}H_{14}O_5$: C 69.67, H 4.55. Found: C 69.69, H 4.58.

6-Methoxy-3-(3′,4′-dimethoxybenzoyl)coumarin (**2**): 97% yield; beige solid; mp 202–203 °C; ^{1}H-NMR (300 MHz, $CDCl_3$) δ ppm 7.78 (s, 1H, H-4), 7.38 (d, *J* = 1.9 Hz, 1H, H-2′), 7.26 (dd, *J* = 8.4, 2.0 Hz, 1H, H-6′), 7.16 (d, *J* = 9.1 Hz, 1H, H-8), 7.04 (dd, *J* = 9.1, 2.9 Hz, 1H, H-7), 6.82 (d, *J* = 2.9 Hz, 1H, H-5), 6.70 (d, *J* = 8.4 Hz, 1H, H-5′), 3.78 (s, 6H, 2x OCH_3), 3.69 (s, 3H, OCH_3); ^{13}C-NMR (75 MHz, $CDCl_3$) δ ppm 190.4, 156.6, 154.4, 149.5, 149.3, 144.4, 129.4, 128.0, 125.7, 121.6, 118.8, 118.2, 111.2, 110.8, 110.2, 56.4, 56.3, 56.1; EI-MS *m*/*z* (%): 341 ([M + 1]$^+$, 58), 340 ([M]$^+$, 94), 165 (100), 77 (22); Anal. Calcd. For $C_{19}H_{16}O_6$: C 67.05, H 4.74. Found: C 67.09, H 4.75.

5,7-Dimethoxy-3-(3′,4′-dimethoxybenzoyl)coumarin (**3**): 91% yield; pale yellow solid; mp 210–211 °C; ^{1}H-NMR (300 MHz, $CDCl_3$) δ ppm 8.19 (s, 1H, H-4), 7.34 (d, *J* = 1.9 Hz, 1H, H-2′), 7.26 (dd, *J* = 8.4, 2.0 Hz, 1H, H-6′), 6.70 (d, *J* = 8.4 Hz, 1H, H-5′), 6.29 (d, *J* = 2.0 Hz, 1H, H-6), 6.14 (d, *J* = 2.0 Hz, 1H, H-8), 3.77 (bs, 6H, 2x OCH_3), 3.72 (bs, 6H, 2x OCH_3); ^{13}C-NMR (75 MHz, $CDCl_3$) δ ppm 190.9, 165.8, 159.4, 158.4, 158.0, 153.9, 149.3, 141.5, 130.0, 125.4, 121.3, 111.5, 110.1, 103.9, 95.4, 93.0, 56.3; EI-MS *m*/*z* (%): 371 ([M + 1]$^+$, 24), 370 (M$^+$, 100), 339 (21), 233 (30), 165 (63); Anal. Calcd. For $C_{20}H_{18}O_7$: C 64.86, H 4.90. Found: C 64.88, H 4.93.

5,7-Dimethoxy-3-(4′-methoxybenzoyl)coumarin (**4**): 97% yield; pale yellow solid; mp 174–175 °C; ^{1}H-NMR (300 MHz, $CDCl_3$) δ ppm 8.21 (s, 1H, H-4), 7.69 (d, *J* = 8.8 Hz, 2H, H-2′, H-6′), 6.77 (d, *J* = 8.8 Hz,

2H, H-3′, H-5′), 6.29 (d, *J* = 2.2 Hz, 1H, H-6), 6.13 (d, *J* = 2.2 Hz, 1H, H-8), 3.72 (2s, 3H + 3H, 2x OCH_3), 3.70 (s, 3H, OCH_3); ^{13}C-NMR (75 MHz, $CDCl_3$) δ ppm 190.7, 165.6, 163.8, 159.1, 158.2, 157.8, 141.5, 132.1, 129.8, 121.2, 113.7, 103.8, 95.2, 92.8, 56.1, 56.0, 55.5; EI-MS *m*/*z* (%): 341 ([M + 1]$^+$, 33), 340 (M$^+$, 88), 325 (28) 312 (30), 309 (45), 297 (20), 233 (48), 135 (100), 92 (27), 77 (38). Anal. Calcd. For $C_{19}H_{16}O_6$: C 67.05, H 4.74. Found: C 67.08, H 4.76.

5,7-Dihydroxy-3-(4′-hydroxybenzoyl)coumarin (**8**): 88% yield; pale green solid; mp 290–292 °C; ^{1}H-NMR (300 MHz, DMSO-d_6) δ ppm 11.10 (s, 1H), 10.85 (s, 1H), 10.53 (s, 1H), 8.09 (d, *J* = 1.4 Hz, 1H), 7.67 (d, *J* = 8.6 Hz, 2H), 6.80 (d, *J* = 8.7 Hz, 2H), 6.25 (d, *J* = 2.0 Hz, 1H), 6.22 (d, *J* = 1.8 Hz, 1H); ^{13}C-NMR (75 MHz, DMSO-d_6) δ ppm 190.4, 164.2, 162.4, 158.8, 157.5, 157.2, 141.1, 132.3, 128.3, 119.0, 115.3, 101.5, 98.5, 94.3. EI-MS *m*/*z* (%): 299 ([M + 1]$^+$, 9), 298 (M$^+$, 31), 283 (16), 218 (20), 121 (100), 93 (26), 65 (27). Anal. Calcd. For $C_{16}H_{10}O_6$: C 64.43, H 3.38. Found: C 64.39, H 3.37.

3.2. Biological Assays

3.2.1. Binding Affinity Assays

The binding affinity for hA$_1$, hA$_{2A}$, hA$_3$ of the synthetized compounds was evaluated using radioligand competition experiments in CHO cells that were stably transfected with the individual receptor subtypes [44,45]. The radioligands used were 1 nM [^{3}H]CCPA for hA$_1$ (K_D = 0.61 nM), 10 nM [^{3}H]NECA for hA$_{2A}$ (K_D = 20.1 nM), and 1 nM [^{3}H]HEMADO for hA$_3$ (K_D = 1.2 nM) receptors. Due to the lack of a suitable radioligand for the hA$_{2B}$ receptor, the potency of antagonists at the hA$_{2B}$ receptor (expressed on CHO cells) was determined by inhibition of NECA-stimulated adenylyl cyclase activity [44,45]. The IC_{50} for inhibition of cAMP (cyclic adenosine monophosphate) production was determined and converted to K_i values using the Cheng and Prusoff equation [56]. For all the tested compounds, no measurable activity for the hA$_{2B}$ (K_i > 10 μM) was detected.

3.2.2. Statistical Methods

K_i values (dissociation constants) were determined in radioligand competition experiments with 7–8 different concentrations of test compound and each concentration was tested in duplicate. K_i values are given as geometric means of three independent experiments with 95% confidence intervals. The program Prism 6 (GraphPad Software) was used for the analysis of the competition curves.

3.3. Theoretical Evaluation of ADME Properties

cLogP was calculated by the methodology developed by Molinspiration as a sum of fragment-based contributions and correction factors. Topological Polar Surface Area (TPSA) was calculated based on the methodology published by Ertl et al. as a sum of fragment contributions [57]. Oxygen- and nitrogen-centered polar fragments are considered. TPSA has been shown to be a very good descriptor characterizing drug absorption, including intestinal absorption, bioavailability, Caco-2 permeability and blood–brain barrier penetration. The method for calculation of molecule volume developed at Molinspiration is based on group contributions. These have been obtained by fitting the sum of fragment contributions to "real" 3D volume for a training set of about twelve thousand, mostly drug-like molecules. Three-dimensional molecular geometries for a training set were fully optimized by the semiempirical AM1 method.

3.4. Molecular Modeling

Homology modeling was carried out using the Molecular Operating Environment (MOE) suite [49]. Molecular docking simulations were performed with the Schrodinger package [51,52].

3.4.1. Homology Models of hA$_1$ and hA$_3$

Homology models of the hA1 and hA$_3$ were constructed. The crystallized structure of the hA$_{2A}$ receptor (PDB: 3EML) was used as a template [48]. Protein sequence alignment of the 3 receptors (hA$_1$, hA$_{2A}$ and hA$_3$) used to generate the homology models was performed as previously described by Katritch et al. [50]. The alignment was made considering the highly conserved residues in the different TM helices. MOE software was used to generate the homology models [49]. Protein geometry was evaluated for the models taking into account Phi–Psi plots, rotamers, bond angles, bond lengths, atom clashes, dihedrals and contact energies. The presence of different conserved disulfide bridges was manually checked, such as the bridge between the corresponding Cys77 and Cys166 residues in the hA$_{2A}$. Induce Fit Docking Workflow in the Schrodinger package was used to optimize the final models [58]. Selective high affinity ligands (compounds coll_11 and jaco_mre3008_f20) [50] were used to adapt the protein pocket for the hA$_1$ and hA$_3$, respectively. This procedure involved three steps: 1) Glide-based docking of the ligands using SP mode (standard-precision); 2) Protein pocket optimization using Prime and considering the residues within 5Å from the ligand poses; 3) Glide-based docking of the ligands in the refined pocket using XP mode (Extra-precision). As previously described [50], homology models were tested for their capability to discriminate ligands from decoys and between known subtype-selective compounds. ROC curves were performed, and the best models were selected for further molecular docking studies.

3.4.2. Molecular Docking of hA$_1$ and hA$_3$ ARs

Molecular docking studies using the hA$_1$ and hA$_3$ homology models, selected in the previous step, were carried out. Compounds were docked using Glide SP mode [52]. Ten poses for each ligand were collected and optimized using MM-GBSA in Prime [53], taking into account a flexible protein region defined by 5 Å from the ligand. Final binding modes were selected, taking into account the number of similar poses extracted from the calculations and geometrical correspondence to co-crystallized ligands in the hA$_{2A}$.

4. Conclusions

The current study was focused on the synthesis and the evaluation of binding affinity towards the four subtypes of human ARs of a selected series of methoxy and hydroxy coumarin–chalcone hybrids. Structure–activity relationship (SAR) studies of the new molecules highlighted that, in general, methoxy substitutions, as in the example of compounds **3** and **4,** allow a superior hA$_3$ binding affinity and selectivity, whereas the hydroxy substitutions, as in the example of compounds **5**–**8**, allow a modest hA$_1$ binding affinity. Substitutions at positions 5 and 7 of the coumarin scaffold proved to be essential for the potency and selectivity in both series of compounds. Compound **4**, a methoxy derivative, and compound **7**, a hydroxy derivative, proved to be the most potent compounds of the studied series, displaying a hA$_3$ K_i = 2.49 μM and a hA$_1$ K_i = 17.7 μM, respectively. Docking calculations allow an understanding the binding preference of the studied molecules. Finally, the theoretical values for the ADME properties show that all the coumarin–chalcone hybrids **1**–**8** do not break any of Lipinski's rules, being promising scaffolds for further compound optimization.

Author Contributions: Conceptualization, S.V.-R. and M.J.M.; methodology, S.V.-R., S.V. and S.K.; software, S.V.; validation, K.-N.K., F.B. and E.U.; formal analysis, S.V.-R., S.K. and S.V.; investigation, S.V.-R., S.K., S.V. and M.J.M.; resources, S.V.-R., S.K., S.V., K.-N.K., E.U., F.B. and M.J.M.; data curation, S.V.-R., S.K., S.V.; writing—original draft preparation and editing, S.V.-R.; writing—review and editing, M.J.M.; visualization, K.-N.K.; supervision, F.B. and E.U.; project administration, S.V.-R. and M.J.M.; funding acquisition, S.V.-R., S.K., S.V., K.-N.K., E.U., F.B. and M.J.M. All authors have read and agreed to the published version of the manuscript.

Funding: This research was funded by Xunta de Galicia (Galician Plan of Research, Innovation and Growth 2011–2015, Plan I2C, ED481B 2014/027-0, ED481B 2014/086–0 and ED481B 2018/007), Angeles Alvariño program from Xunta de Galicia, European Social Fund (ESF) and Fundação para a Ciência e Tecnologia (FCT, CEECIND/02423/2018 and UIDB/00081/2020).

Acknowledgments: The authors would like to thank Lourdes Santana for her scientific support. The authors would like to thank the use of RIAIDT-USC analytical facilities.

Conflicts of Interest: The authors declare no conflict of interest.

References

1. Fredholm, B.B.; IJzerman, A.P.; Jacobson, K.A.; Linden, J.; Müller, C.E. International union of basic and clinical pharmacology. LXXXI. Nomenclature and classification of adenosine receptors-an update. *Pharmacol. Rev.* **2011**, *63*, 1–34. [CrossRef] [PubMed]
2. Poulsen, S.A.; Quinn, R.J. Adenosine receptors: New opportunities for future drugs. *Bioorg. Med. Chem.* **1998**, *6*, 619–641. [CrossRef]
3. Fredholm, B.B.; IJzerman, A.P.; Jacobson, K.A.; Klotz, K.N.; Linden, J. International union of pharmacology. XXV. Nomenclature and classification of adenosine receptors. *Pharmacol. Rev.* **2001**, *5*, 527–552.
4. Fredholm, B.B.; Arslan, G.; Halldner, L.; Kull, B.; Schulte, G.; Wasserman, W. Structure and function of adenosine receptors and their genes. *Arch. Pharmacol.* **2000**, *362*, 364–374. [CrossRef] [PubMed]
5. Draper-Joyce, C.J.; Khoshouei, M.; Thal, D.M.; Liang, Y.-L.; Nguyen, A.T.N.; Furness, S.G.B.; Venugopal, H.; Baltos, J.-A.; Plitzko, J.M.; Danev, R.; et al. Structure of the adenosine-bound human adenosine A1 receptor-Gi complex. *Nature* **2018**, *558*, 559–563. [CrossRef] [PubMed]
6. Zhou, Q.Y.; Li, C.; Olah, M.E.; Johnson, R.A.; Stiles, G.L.; Civelli, O. Molecular cloning and characterization of an adenosine receptor: The A3 adenosine receptor. *Proc. Natl. Acad. Sci. USA* **1992**, *89*, 7432–7436. [CrossRef]
7. Salvatore, C.A.; Jacobson, M.A.; Taylor, H.E.; Linden, J.; Johnson, R.G. Molecular cloning and characterization of the human A_3 adenosine receptor. *Proc. Natl. Acad. Sci. USA* **1993**, *90*, 10365–10369. [CrossRef]
8. Ramkumar, V.; Stiles, G.L.; Beaven, M.A.; Ali, H. The A_3 adenosine receptor is the unique adenosine receptor which facilitates release of allergic mediators in mast cells. *J. Biol. Chem.* **1993**, *268*, 16887–16890.
9. Linden, J. Cloned adenosine A_3 receptors: Pharmacological properties, species differences and receptor functions. *Trends Pharmacol. Sci.* **1994**, *15*, 298–306. [CrossRef]
10. Hannon, J.P.; Pfannkuche, H.J.; Fozard, J.R. A role for mast cells in adenosine A_3 receptor-mediated hypotension in the rat. *J. Pharmacol.* **1995**, *115*, 945–952. [CrossRef]
11. Jacobson, K.A.; Nikodijević, O.; Shi, D.; Gallo-Rodriguez, C.; Olah, M.E.; Stiles, G.L.; Daly, J.W. A role for central A_3-adenosine receptors. Mediation of behavioral depressant effects. *FEBS Lett.* **1993**, *336*, 57–60. [CrossRef]
12. Vecchio, E.A.; Baltos, J.A.; Nguyen, A.T.N.; Christopoulos, A.; White, P.J.; May, L.T. New paradigms in adenosine receptor pharmacology: Allostery, oligomerization and biased agonism. *Br. J. Pharmacol.* **2018**, *175*, 4036–4046. [CrossRef] [PubMed]
13. Kim, Y.; de Castro, S.; Gao, Z.G.; IJzerman, A.P.; Jacobson, K.A. Novel 2- and 4-substituted 1*H*-imidazo [4,5-*c*]quinolin-4-amine derivatives as allosteric modulators of the A_3 adenosine receptor. *J. Med. Chem.* **2009**, *52*, 2098–2108. [CrossRef] [PubMed]
14. Lopes, L.V.; Sebastião, A.M.; Ribeiro, J.A. Adenosine and related drugs in brain diseases: Present and future in clinical trials. *Curr. Top. Med. Chem.* **2011**, *11*, 1087–1101. [CrossRef]
15. Jespers, W.; Schiedel, A.C.; Heitman, L.H.; Cooke, R.M.; Kleene, L.; van Westen, G.J.P.; Gloriam, D.E.; Müller, C.E.; Sotelo, E.; Gutiérrez-de-Terán, H. Structural mapping of adenosine receptor mutations: Ligand binding and signaling mechanisms. *Trends Pharmacol. Sci.* **2018**, *39*, 75–89. [CrossRef]
16. Shah, R.H.; Frishmanet, W.H. Adenosine1 receptor antagonism: A new therapeutic approach for the treatment of decompensated heart failure. *Cardiol. Rev.* **2009**, *17*, 125–131. [CrossRef]
17. Shook, B.; Rassnick, S.; Wallace, N.; Crooke, J.; Ault, M.; Chakravarty, D.; Barbay, J.K.; Wang, A.; Powell, M.T.; Leonard, K.; et al. Design and characterization of optimized adenosine A_{2A}/A_1 receptor antagonists for the treatment of Parkinson's disease. *J. Med. Chem.* **2012**, *55*, 1402–1417. [CrossRef]
18. Liu, Y.J.; Chen, J.; Li, X.; Zhou, X.; Hu, Y.M.; Chu, S.F.; Peng, Y.; Chen, N.H. Research progress on adenosine in central nervous system diseases. *CNS Neurosci. Ther.* **2019**, *25*, 899–910. [CrossRef]
19. Stone, T.W.; Ceruti, S.; Abbracchio, M.P. Adenosine receptors and neurological disease: Neuroprotection and neurodegeneration. *Handb. Exp. Pharmacol.* **2009**, *193*, 535–587.
20. Wilcox, C.S.; Welch, W.J.; Schreiner, G.F.; Belardinelli, L. Natriuretic and diuretic actions of a highly selective adenosine receptor antagonist. *J. Am. Soc. Nephrol.* **1999**, *10*, 714–720.

21. Gottlieb, S.S.; Skettino, S.L.; Wolff, A.; Beckman, E.; Fisher, M.L.; Freudenberger, R.; Gladwell, T.; Marshall, J.; Cines, M.; Bennett, D.; et al. Effects of BG9719 (CVT-124), an A_1 adenosine receptor antagonist, and Furosemide on glomerular filtration rate and natriuresis in patients with congestive heart failure. *J. Am. Coll. Cardiol.* **2000**, *35*, 56–59. [CrossRef]
22. de Mendonça, A.; Sebastião, A.M.; Ribeiro, J.A. Adenosine: Does it have a neuroprotective role after all? *Brain Res. Rev.* **2000**, *33*, 258–274. [CrossRef]
23. Lee, H.T.; Ota-Setlik, A.; Xu, H.; D'Agati, V.D.; Jacobson, M.A.; Emala, C.W. A_3 adenosine receptor knockout mice are protected against ischemia- and myoglobinuria-induced renal failure. *Am. J. Physiol. Renal Physiol.* **2003**, *284*, 267–273. [CrossRef]
24. Kolahdouzan, M.; Hamadeh, M.J. The neuroprotective effects of caffeine in neurodegenerative diseases. *CNS Neurosci. Ther.* **2017**, *23*, 272–290. [CrossRef]
25. Pugliese, A.M.; Coppi, E.; Spalluto, G.; Corradetti, R.; Pedata, F. A_3 adenosine receptor antagonists delay irreversible synaptic failure caused by oxygen and glucose deprivation in the rat CA_1 hippocampus in vitro. *Br. J. Pharmacol.* **2006**, *147*, 524–532. [CrossRef]
26. Fishman, P.; Bar-Yehuda, S.; Liang, B.T.; Jacobson, K.A. Pharmacological and therapeutic effects of A_3 adenosine receptor (A_3AR) agonists. *Drug Discov. Today* **2012**, *17*, 359–366. [CrossRef]
27. Chen, Z.; Janes, K.; Chen, C.; Doyle, T.; Tosh, D.K.; Jacobson, K.A.; Salvemini, D. Controlling murine and rat chronic pain through A_3 adenosine receptor activation. *FASEB J.* **2012**, *26*, 1855–1865. [CrossRef]
28. Baraldi, P.G.; Tabrizi, M.A.; Gessi, S.; Borea, P.A. Adenosine receptor antagonists: Translating medicinal chemistry and pharmacology into clinical utility. *Chem. Rev.* **2008**, *108*, 238–263. [CrossRef]
29. Moro, S.; Gao, Z.G.; Jacobson, K.A.; Spalluto, G. Progress in the pursuit of therapeutic adenosine receptor antagonists. *Med. Res. Rev.* **2006**, *26*, 131–159. [CrossRef]
30. Okajima, F.; Akbar, M.; Abdul Majid, M.; Sho, K.; Tomura, H.; Kondo, Y. Genistein, an inhibitor of protein tyrosine kinase, is also a competitive antagonist for P1-purinergic (adenosine) receptor in FRTL-5 thyroid cells. *Biochem. Biophys. Res. Commun.* **1994**, *203*, 1488–1495. [CrossRef]
31. Jacobson, K.A.; Moro, S.; Manthey, J.A.; West, P.L.; Ji, X.D. Interactions of flavones and other phytochemicals with adenosine receptors. *Adv. Exp. Med. Biol.* **2002**, *505*, 163–171.
32. Borges, F.; Roleira, F.; Milhazes, N.; Santana, L.; Uriarte, E. Simple coumarins and analogues in medicinal chemistry: Occurrence, synthesis and biological activity. *Curr. Med. Chem.* **2005**, *12*, 887–916. [CrossRef]
33. Go, M.L.; Wu, X.; Liu, X.L. Chalcones: An update on cytotoxic and chemoprotective properties. *Curr. Med. Chem.* **2005**, *12*, 483–499. [CrossRef]
34. Nowakowska, Z. A review of anti-infective and anti-inflammatory chalcones. *Eur. J. Med. Chem.* **2007**, *42*, 125–137. [CrossRef]
35. Langmead, C.J.; Andrews, S.P.; Congreve, M.; Errey, J.C.; Hurrell, E.; Marshall, F.H.; Mason, J.S.; Richardson, C.M.; Robertson, N.; Zhukov, A.; et al. Identification of novel adenosine $A_{(2A)}$ receptor antagonists by virtual screening. *J. Med. Chem.* **2012**, *55*, 1904–1909. [CrossRef]
36. Vazquez-Rodriguez, S.; Matos, M.J.; Santana, L.; Uriarte, E.; Borges, F.; Kachler, S.; Klotz, K.N. Chalcone-based derivatives as new scaffolds for hA_3 adenosine receptor antagonists. *J. Pharm. Pharmacol.* **2013**, *65*, 607–703. [CrossRef]
37. Gaspar, A.; Reis, J.; Matos, M.J.; Uriarte, E.; Borges, F. In search for new chemical entities as adenosine receptor ligands: Development of agents based on benzo-γ-pyrone skeleton. *Eur. J. Med. Chem.* **2012**, *54*, 914–918. [CrossRef]
38. Matos, M.J.; Vilar, S.; Vazquez-Rodriguez, S.; Kachler, S.; Klotz, K.N.; Buccioni, M.; Delogu, G.; Santana, L.; Uriarte, E.; Borges, F. Structure-based optimization of coumarin hA_3 adenosine receptor antagonists. *J. Med. Chem.* **2020**, *63*, 2577–2587. [CrossRef]
39. Matos, M.J.; Vilar, S.; Kachler, S.; Fonseca, A.; Santana, L.; Uriarte, E.; Borges, F.; Tatonetti, N.P.; Klotz, K.N. Insight into the interactions between novel coumarin derivatives and human A_3 adenosine receptors. *ChemMedChem* **2014**, *9*, 2245–2253. [CrossRef]
40. Matos, M.J.; Vilar, S.; Kachler, S.; Celeiro, M.; Vazquez-Rodriguez, S.; Santana, L.; Uriarte, E.; Hripcsak, G.; Borges, F.; Klotz, K.N. Development of novel adenosine receptor ligands based on the 3-amidocoumarin scaffold. *Bioorg. Chem.* **2015**, *61*, 1–6. [CrossRef]

41. Matos, M.J.; Vilar, S.; Kachler, S.; Vazquez-Rodriguez, S.; Varela, C.; Delogu, G.; Hripcsak, G.; Santana, L.; Uriarte, E.; Klotz, K.N.; et al. Progress in the development of small molecules as new human A_3 adenosine receptor ligands based on the 3-thiophenylcoumarin core. *MedChemComm* **2016**, *7*, 845–852. [CrossRef]
42. Fonseca, A.; Matos, M.J.; Vilar, S.; Kachler, S.; Klotz, K.N.; Uriarte, E.; Borges, F. Coumarins and adenosine receptors: New perceptions in. structure–affinity relationships. *Chem. Biol. Drug Des.* **2018**, *91*, 245–256. [CrossRef]
43. Vazquez-Rodriguez, S.; Figueroa-Guiñez, R.; Matos, M.J.; Santana, L.; Uriarte, E.; Lapier, M.; Maya, J.D.; Olea-Azar, C. Synthesis of coumarin–chalcone hybrids and evaluation of their antioxidant and trypanocidal properties. *Med. Chem. Commun.* **2013**, *4*, 993–1000. [CrossRef]
44. Klotz, K.N.; Hessling, J.; Hegler, J.; Owman, C.; Kull, B.; Fredholm, B.B.; Lohse, M.J. Comparative pharmacology of human adenosine receptor subtypes-characterization of stably transfected receptors in CHO cells. *Arch. Pharmacol.* **1997**, *357*, 1–9. [CrossRef]
45. Klotz, K.N.; Falgner, N.; Kachler, S.; Lambertucci, C.; Vittori, S.; Volpini, R.; Cristalli, G. [3H]HEMADO–a novel tritiated agonist selective for the human adenosine A_3 receptor. *Eur. J. Pharmacol.* **2007**, *556*, 14–18. [CrossRef]
46. M cheminformatics, Bratislava, Slovak Republic. 2009. Available online: http://www.molinspiration.com/services/properties.html (accessed on 19 September 2020).
47. Irwin, J.J.; Shoichet, B.K. ZINC–a free database of commercially available compounds for virtual screening. *J. Chem. Inf. Model.* **2005**, *45*, 177–182. [CrossRef]
48. Jaakola, V.P.; Griffith, M.T.; Hanson, M.A.; Cherezov, V.; Chien, E.Y.; Lane, J.R.; Ijzerman, A.P.; Stevens, R.C. The 2.6 angstrom crystal structure of a human A_{2A} adenosine receptor bound to an antagonist. *Science* **2008**, *322*, 1211–1217. [CrossRef]
49. *MOE, Version 2011.10*; Chemical Computing Group, Inc.: Montreal, QC, Canada, 2011.
50. Katritch, V.; Kufareva, I.; Abagyan, R. Structure based prediction of subtype-selectivity for adenosine receptor antagonists. *Neuropharmacology* **2011**, *60*, 108–115. [CrossRef]
51. *Glide, Version 5.7*; Schrödinger, LLC: New York, NY, USA, 2011.
52. *Prime, Version 3.0*; Schrödinger, LLC: New York, NY, USA, 2011.
53. Congreve, M.; Andrews, S.P.; Doré, A.S.; Hollenstein, K.; Hurrell, E.; Langmead, C.J.; Mason, J.S.; Ng, I.W.; Tehan, B.; Zhukov, A.; et al. Discovery of 1,2,4-triazine derivatives as adenosine $A_{(2A)}$ antagonists using structure based drug design. *J. Med. Chem.* **2012**, *55*, 1898–1903. [CrossRef]
54. Lenzi, O.; Colotta, V.; Catarzi, D.; Varano, F.; Poli, D.; Filacchioni, G.; Varani, K.; Vincenzi, F.; Borea, P.A.; Paoletta, S.; et al. 2-Phenylpyrazolo[4,3-*d*]pyrimidin-7-one as a new scaffold to obtain potent and selective human A_3 adenosine receptor antagonists: New insights into the receptor-antagonist recognition. *J. Med. Chem.* **2009**, *52*, 7640–7652. [CrossRef]
55. Gaspar, A.; Reis, J.; Kachler, S.; Paoletta, S.; Uriarte, E.; Klotz, K.N.; Moro, S.; Borges, F. Discovery of novel A_3 adenosine receptor ligands based on chromone scaffold. *Biochem. Pharmacol.* **2012**, *84*, 21–29. [CrossRef] [PubMed]
56. Cheng, Y.; Prusoff, W.H. Relationship between the inhibition constant (K_1) and the concentration of inhibitor which causes 50 per cent inhibition (IC_{50}) of an enzymatic reaction. *Biochem. Pharmacol.* **1973**, *22*, 3099–3108. [PubMed]
57. Ertl, P.; Rohde, B.; Selzer, P. Fast calculation of molecular polar surface area as a sum of fragment-based contributions and its application to the prediction of drug transport properties. *J. Med. Chem.* **2000**, *43*, 3714–3717. [CrossRef] [PubMed]
58. Sherman, W.; Day, T.; Jacobson, M.P.; Friesner, R.A.; Farid, R. Novel procedure for modeling ligand/receptor induced fit effects. *J. Med. Chem.* **2006**, *49*, 534–553. [CrossRef] [PubMed]

Sample Availability: Samples of the compounds are available from the authors.